

Diagnosing Moisture Sources for Flash Floods in the United States. Part II: Terrestrial and Oceanic Sources of Moisture

JESSICA M. ERLINGIS

Cooperative Institute for Mesoscale Meteorological Studies, and School of Meteorology, University of Oklahoma, and NOAA/National Severe Storms Laboratory, Norman, Oklahoma

JONATHAN J. GOURLEY

NOAA/National Severe Storms Laboratory, and School of Meteorology, University of Oklahoma, Norman, Oklahoma

JEFFREY B. BASARA

School of Meteorology, and School of Civil Engineering and Environmental Science, University of Oklahoma, Norman, Oklahoma

(Manuscript received 6 June 2018, in final form 1 May 2019)

ABSTRACT

Backward trajectories were derived from North American Regional Reanalysis data for 19 253 flash flood reports published by the National Weather Service to determine the along-path contribution of the land surface to the moisture budget for flash flood events in the conterminous United States. The impact of land surface interactions was evaluated seasonally and for six regions: the West Coast, Arizona, the Front Range, Flash Flood Alley, the Missouri Valley, and the Appalachians. Parcels were released from locations that were impacted by flash floods and traced backward in time for 120 h. The boundary layer height was used to determine whether moisture increases occurred within the boundary layer or above it. Moisture increases occurring within the boundary layer were attributed to evapotranspiration from the land surface, and surface properties were recorded from an offline run of the Noah land surface model. In general, moisture increases attributed to the land surface were associated with anomalously high surface latent heat fluxes and anomalously low sensible heat fluxes (resulting in a positive anomaly of evaporative fraction) as well as positive anomalies in top-layer soil moisture. Over the ocean, uptakes were associated with positive anomalies in sea surface temperatures, the magnitude of which varies both regionally and seasonally. Major oceanic surface-based source regions of moisture for flash floods in the United States include the Gulf of Mexico and the Gulf of California, while boundary layer moisture increases in the southern plains are attributable in part to interactions between the land surface and the atmosphere.

1. Introduction

The land surface is linked to the atmosphere through exchanges of energy, carbon, and moisture that occur within the planetary boundary layer (PBL), and such linkages have been studied from scales ranging from the microscale to the climate scale. At climate scales, modeling studies delineate regions where feedback

mechanisms between soil moisture availability and precipitation occur (Koster et al. 2004; Luo et al. 2007). Such studies, however, oftentimes focus on coupling on a local or basin scale, without considering the effects of advection.

Surface fluxes can affect precipitation patterns by modulating boundary layer temperature and moisture profiles (Ek and Mahrt 1994; Findell and Eltahir 2003). Such interactions have varying effects and can induce positive and negative feedback loops. For example, evaporation can moisten the boundary layer sufficiently, lowering the lifting condensation level so that clouds form, precipitation occurs, and the cycle repeats itself. Another possibility is that large sensible heat fluxes from dry soils can cause an increase in parcel buoyancy,

Supplemental information related to this paper is available at the Journals Online website: <https://doi.org/10.1175/JHM-D-18-0120.s1>.

Corresponding author: Jessica M. Erlingis, jessica.erlingislamers@nasa.gov

DOI: 10.1175/JHM-D-18-0120.1

© 2019 American Meteorological Society. For information regarding reuse of this content and general copyright information, consult the [AMS Copyright Policy](#) (www.ametsoc.org/PUBSReuseLicenses).

allowing parcels to rise sufficiently to reach their level of free convection.

Furthermore, land surface cover and/or states can have an effect on the properties of downstream precipitation (Mo et al. 1997; Erlingis and Barros 2014) by modifying an air mass through energy and moisture exchanges with the surface. Given that land–atmosphere interactions can have such a nonlocal effect, trajectories are a useful tool for assessing how the surface may modify the water budget of air parcels that lead to an event of interest, specifically flash flood events in this study.

Previous studies have used trajectories to investigate the water budget at both climate and event scales [see Gimeno et al. (2012) for a comprehensive review]. At the climate scale, Stohl and James (2004, 2005) used the Lagrangian particle dispersion model FLEXPART to study the global distribution of annual mean freshwater surface flux by assessing residual of evapotranspiration and precipitation. Nieto et al. (2006) adopted their methodology and used European Centre for Medium-Range Forecasts (ECMWF) data and the FLEXPART model (Stohl and James 2004, 2005) to diagnose moisture sources for the Sahel region. Drumond et al. (2008) applied the same methodology for central Brazil and the La Plata basin, while Sun and Wang (2014) identified moisture sources for grasslands in China. Sorí et al. (2015) employed trajectories to assess the contribution of the Atlantic warm pool to the hydrological budget of Central and North America.

Dirmeyer and Brubaker (1999, 2007), Brubaker et al. (2001), and Dirmeyer and Kinter (2010) applied a different method to analyzing water budgets using hourly observed precipitation data, reanalysis data, and a quasi-isentropic backward trajectory algorithm. In this algorithm, the height of a parcel is determined by its potential temperature, and winds are used for advection. They launch parcels backward in time from grid boxes where precipitation occurred at a rate proportional to the precipitation rate and distribute the parcels vertically based on a water-mass-weighted random sample. The above methodology was used to quantify the seasonal precipitation recycling ratio worldwide and also to identify long-term moisture sources for floods of interest in the Midwest.

Other methodologies include tracing water vapor within the Weather Research and Forecasting (WRF) Model, as in Dominguez et al. (2016), which was used to estimate both local precipitation recycling and water vapor transport in a forward model for the North American monsoon region. Arnault et al. (2016) and Wei et al. (2016) used a tracer method (called e-tagging) in a forward model to assess the precipitation recycling ratio and the atmospheric water vapor residence time, respectively.

Sodemann et al. (2008) expanded upon the work by Stohl and James (2004, 2005) to assess the moisture sources for precipitation in Greenland under different phases of the North Atlantic Oscillation (NAO), not only by their geographical locations, but by their locations within an atmospheric column. They ascribe the increases in parcel moisture to the PBL or to outside of the PBL. The application of their methodology is discussed in further detail in section 2.

Previous work has used backward trajectories to assess the differences in precipitation and evaporation along parcel trajectories for case studies or seasonally for all rainfall events. In this study, the method is adapted and applied to thousands of flash flood events. The hypotheses of this study are twofold: 1) if land–atmosphere interactions have an effect on the water budget, then it is a positive contribution for flash flood–producing storms (i.e., the moisture for flood events is not solely advected) and 2) if the prior hypothesis is true, then importance of the land surface to a flash flood event varies both seasonally and regionally.

The companion manuscript to this paper (Erlingis et al. 2019, hereafter Part I) introduced the study domain, the flash flood database used, and the regions of interest. Kinematic trajectories were produced for 19253 flood events and presented as they relate to the regional and seasonal mechanisms for producing heavy rainfall and flash flooding in the United States. In this manuscript, the moisture budget along the trajectories is analyzed along with the modeled state of the land surface when moisture increases occur.

2. Methodology

The trajectories calculated from NARR data and presented in Part I of this manuscript are used in this study along with a retrospective run of the High-Resolution Land Data Assimilation System (HRLDAS; Chen et al. 2007). HRLDAS was developed at the National Center for Atmospheric Research (NCAR) to run the Noah land surface model (LSM), which evolved from the Oregon State University model (Pan and Mahrt 1987; Chen and Dudhia 2001; Ek et al. 2003) separately, or uncoupled, from the atmospheric component of the WRF Model (Skamarock et al. 2008). Land surface models can be used to study land surface processes uncoupled from the atmosphere or to spinup the soil state variables (temperature, moisture, etc.) at the same grid spacing as a pending coupled numerical weather prediction simulation, where the runs share the same grid spacing, nesting, and land and soil physical properties.

To examine land–atmosphere interactions at scales finer than that of the NARR data, an offline HRLDAS

simulation was conducted. Land surface properties were initialized with USGS land use data and STATSGO soil texture data, and four soil layers were used: 0–10, 10–40, 40–100, and 100–200 cm below ground. A 12-yr retrospective run (2002–13) was conducted using HRLDAS forced by NARR data on the model domain shown in the figures throughout this manuscript, so that flash flood reports in 2007 and beyond had a minimum of ~5 years of soil state spinup. Nemunaitis-Berry et al. (2017) showed that 5 years of spinup was necessary to reach a rough equilibrium state in soil moisture near Oklahoma City, though soil temperature spun up in about 2 years. The Noah land surface model is shown to capture anomaly information well but does have some bias varies with depth, region, and seasonally (Xia et al. 2013). As with all land surface models, sources of uncertainty in addition to model structure and forcing include soil and vegetation parameters (Robock et al. 2003).

The framework for analyzing each event is largely based on the work of Sodemann et al. (2008) who performed an analysis of moisture sources for Greenland based on seasonality and phase of the NAO. If liquid water and ice are ignored, then the water budget in an atmospheric column is expressed in an Eulerian framework as (Trenberth and Guillemot 1998)

$$\frac{\partial w}{\partial t} + \nabla \cdot \frac{1}{g} \int_0^{p_s} q \mathbf{v} dp = E - P, \quad (1)$$

where E and P are evaporation and precipitation rates per unit area, $E - P$ is the surface freshwater flux, t is time, g is gravitational acceleration, \mathbf{v} is the horizontal wind, q is specific humidity, p_s is the surface pressure, and w is the precipitable water defined as

$$w = \frac{1}{g} \int_0^{p_s} q dp. \quad (2)$$

Following this framework, the aforementioned studies follow a parcel's trajectory (Stohl and James 2004)

$$\frac{d\mathbf{x}}{dt} = \mathbf{U}[\mathbf{x}(t)], \quad (3)$$

where \mathbf{x} is the particle's position and $\mathbf{U}[\mathbf{x}(t)]$ is the particle's three-dimensional velocity. If specific humidity, q , is interpolated to the parcel's trajectory, then the net rate of change of the water vapor content of the particle (in a Lagrangian framework) is

$$e - p = m \frac{dq}{dt}, \quad (4)$$

where the e and p are rates of moisture increase and decrease along the trajectory and m is the mass of the air

parcel. By summing the net changes of each parcel at each grid point, the total surface freshwater flux is approximated over an area A as

$$E - P \approx \frac{\sum_{k=1}^K (e - p)}{A}, \quad (5)$$

where K is the total number of particles in A . The quantity $E - P$ can then be averaged over time to avoid effects of cloud formation, which would affect the estimates of averages of E or P individually (Stohl and James 2004).

Sodemann et al. (2008) note that other approaches in the literature that use the above framework as their foundation either do not employ kinematic trajectories or diagnose changes in humidity without denoting the parcels' positions in the atmospheric column. In these other frameworks, the sources of evaporation may be quite far from the parcels. To overcome these shortcomings, the following methodology considers the moisture source by noting the parcel's position relative to the top of the PBL.

An example diagram for a conceptual parcel is shown in Fig. 1. Following Sodemann et al. (2008) the change in specific humidity q along an air parcel's trajectory is given by

$$\Delta q^0(t) = q[\mathbf{x}(t)] - q[\mathbf{x}(t - 3\text{h})], \quad (6)$$

where $\mathbf{x}(t)$ refers to the parcel's position at time t . A moisture increase, for example at $t = -72\text{h}$ results in $\Delta q^0(t) > 0$, while a moisture decrease ($t = -60\text{h}$) results in $\Delta q^0(t) < 0$. If the moisture increase occurs when the parcel's height is less than that of the PBL top (e.g., at $t = -72\text{h}$), then the source of the increase is diagnosed as within the boundary layer and ascribed to processes happening at the land surface, such as evapotranspiration. If the moisture increase happens when the parcel's height is greater than that of the PBL top (at $t = -36\text{h}$), the source is designated as a nonboundary layer source. To mitigate these effects, a maximum of 3h preceding the flood were not used in calculating the total moisture uptakes at a given location. That is, the parcels were launched at the nearest 3-h NARR analysis preceding the flood start time recorded in the flood report.

An advantage of this methodology is that the amount of each parcel's final specific humidity can be quantified. Beginning at the point at $t = -120\text{h}$ and proceeding forward in time, the fractional contribution f_n of an uptake at location n occurring within the boundary layer is given by

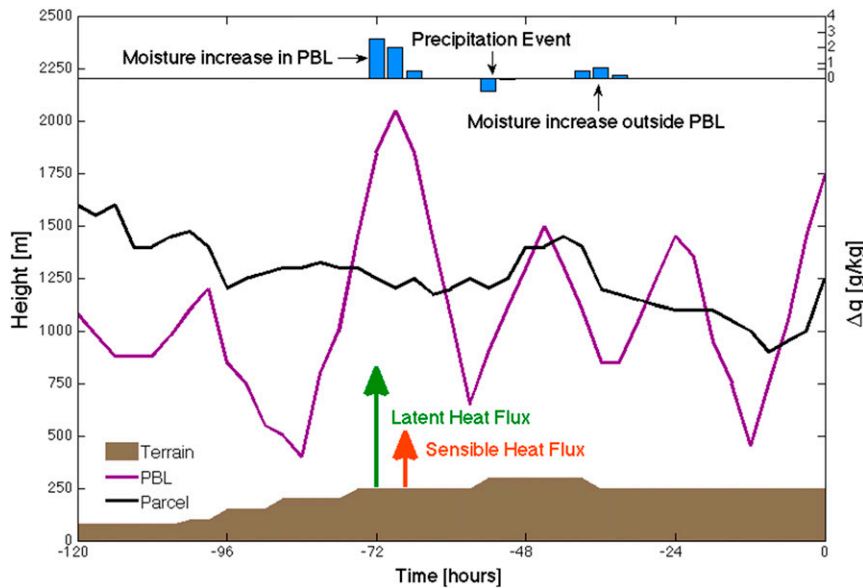


FIG. 1. Conceptual parcel trajectory. Change in parcel water vapor mixing ratio (blue), terrain (brown), PBL height (purple), and parcel height (black) along the trajectory. Adapted from Sodemann et al. (2008).

$$f_n = \frac{\Delta q_n}{q_n}, \quad (7)$$

where Δq_n is the change in specific humidity and q_n is the specific humidity of the air parcel. Each moisture uptake reduces the importance of previous uptake, q_m , so the fractional uptakes are adjusted according to

$$f_m = \frac{\Delta q_m}{q_n}, \quad m > n. \quad (8)$$

When a precipitation event occurs, all previous uptakes are adjusted according to the amount of the moisture decrease (Δq_n^0) as

$$\Delta q'_m = \Delta q_m + \Delta q_n^0 \Delta f_m, \quad m > n. \quad (9)$$

At the end of the parcel's trajectory, the total fractions f_m are summed as to the parcel's location in or above the boundary layer. This produces values of f_{tot} , the total fraction of the final moisture due to boundary layer uptakes, e_{tot} , the total fraction of the final moisture due to nonboundary layer uptakes, and d_{tot} , the total fraction of the final moisture due to uptakes which cannot be classified by this method and are attributed to a variety of causes, such as being preexisting moisture within the parcel (the contribution of moisture advection) or being uptakes smaller than a specified threshold.

The locations of increases in parcel specific humidity were located using the methodology described in this

section. For each region and season, the total boundary layer and nonboundary layer moisture uptakes (increases in specific humidity) are analyzed. Moisture increases were integrated from individual parcel changes in specific humidity according to the adaptation of Sodemann et al. [2008, their Eq. (3)]:

$$Q_{\text{tot}} = \frac{1}{g} \sum_{j=1}^{j=N} \Delta q_j \times 10^{-3} \times \Delta p_j \quad (\text{mm}), \quad (10)$$

where Q_{tot} is the total contribution from either the boundary layer or above the boundary layer, g is the acceleration due to gravity, Δq_j is the change in parcel specific humidity (in g kg^{-1}) for each uptake j (in the total number of uptakes N), and Δp_j is the vertical extent of the air parcel (in Pa).

While this methodology addresses some shortcomings in other methodologies, it does not come without its own drawbacks. It is conceivable that local low-level advection from regions other than along the parcels' track could contribute to increases in moisture within the PBL and are classified as positive contributions from the land surface. For the purposes of this study, this effect is not considered directly but is an area of future research. Nonboundary layer sources of moisture include, but are not limited to, evaporation into the column from precipitation, local advection above the boundary layer, or vertical transport from convection, the last of which is difficult to assess given the velocities at the horizontal grid spacing of the NARR data.

3. Results

a. Spatial and temporal patterns of moisture increases

The total moisture uptake calculated using Eq. (10) (in mm) is presented for each region and season in Figs. 2–7 (note the difference in color bar for each region to highlight areas of importance). For Region 1 (West Coast), boundary layer and nonboundary layer moisture sources are identified over the Pacific Ocean (Fig. 2). In March–May (MAM), there is a small amount of boundary layer moisture uptakes in Northern California as well. In June–August (JJA), slight boundary layer uptakes occur over much of the western United States, though the largest integrated uptakes are over the Gulf of California as a result of the North American monsoon. In September–November (SON), both boundary layer and nonboundary layer uptakes occur broadly over the western United States.

For Region 2 (Fig. 3), the clear source of boundary layer moisture increases during the monsoon season (JJA and SON) is the Gulf of California. Nonboundary layer moisture uptakes occur for the same period in Baja California and along the Mexican coast, as well as within the Gulf of California. Boundary layer contributions slightly outweigh nonboundary layer sources, again highlighting the important role of evaporation from the Gulf of California for air parcels advecting northward during the monsoon. In later sections, we elucidate the relative roles of moisture contribution from the land surface versus the Gulf of California. During December–February (DJF), there are slight increases due to both boundary layer and nonboundary layer sources over the Pacific Ocean. Contributions over land indicate local precipitation recycling, which was estimated to be between 15% and 25% based on the NARR climatology (Dominguez et al. 2008; Hu and Dominguez 2015).

For Region 3 (Front Range), small boundary layer and nonboundary uptakes occur over the Gulf of Mexico and over Texas, New Mexico, and Arizona (Fig. 4). In JJA, there is evidence of contribution of monsoon effects, with the Gulf of California being a source of boundary layer moisture. Additionally, sources of moisture from the land surface appear to occur locally during JJA, with much of Colorado and New Mexico being a hotspot for boundary layer uptakes. Nonboundary layer uptakes also occur in Colorado, New Mexico, and though western Texas, though they are of lesser magnitude (domain median 1.01 mm) than the boundary layer uptakes (domain median 1.96 mm). During SON, boundary layer uptakes occur over the Gulf of Mexico, in western Texas, and in New Mexico and Colorado. Nonboundary layer uptakes also occur in these areas, though the maximum for those contributions is in far southern Texas.

The most important source of boundary layer moisture uptakes is the Gulf of Mexico for Flash Flood Alley (Fig. 5). In the spring, moisture uptakes occur along the preferred flow path of parcels, that is, the northern and central parts of the Gulf of Mexico. The largest cumulative moisture increases occur just before the parcels make landfall along the coast of southeast Texas. In the summer (JJA), there is a larger contribution relative to spring and fall from the area south of Cuba, but the bulk of the moisture gained by parcels during JJA occurs in the western Gulf of Mexico and as parcels approach the Texas coast and over land in south central Texas, where some precipitation recycling may be occurring. Fall moisture uptakes occur in a similar pattern to the spring uptakes for this region. Nonboundary layer moisture for Flash Flood Alley occurs in smaller magnitudes over the western Gulf of Mexico in MAM, but most of the mass gained from parcels above the boundary layer occurs as the parcels make landfall over Texas. The same is true for JJA; the bulk of increases occur as the parcels are nearing the Texas coast or are over Texas. The mass of parcels is increased most over south Texas in SON.

For flash floods occurring over the Missouri Valley, parcels again have boundary layer sources of moisture within the Gulf of Mexico (Fig. 6). However, the maximum value for spring mass uptakes occurs along the Texas coastline, with eastern Texas, eastern Arkansas, and Louisiana, all being key moisture sources for floods in this region. This is likely due to the amount of vegetation that begins to grow in this region in the spring (coincident with the maxima in monthly maps of LAI, shown in Fig. S18 in the online supplemental material). In addition, the maximum mass uptakes for JJA for the Missouri Valley occur onshore in eastern Texas and Oklahoma into Kansas. Broadly, the southern Great Plains has been identified as a region where land–atmosphere coupling plays an important role for precipitation episodes at the climate scale (Koster et al. 2004; Luo et al. 2007) and is also a region where moisture is transported northward via the LLJ (Higgins et al. 1997; Berg et al. 2015; Gimeno et al. 2016). Because there are fewer events in SON for this region, less water vapor is added to parcels in aggregate, but the area with the largest integrated boundary layer uptakes is again in the northern Gulf of Mexico and into Louisiana and Arkansas.

Nonboundary layer uptakes for Region 5 (Missouri Valley) have two regions where they are maximized in MAM. There is a broad area over the Gulf of Mexico with small contributions, but there are maxima located along the Mexican coast and in southwest Oklahoma. In JJA, again the maxima are near Corpus Christi, Texas, and north-central Oklahoma and south-central Kansas. In the fall, there is a broad area of nonboundary layer

Region 1

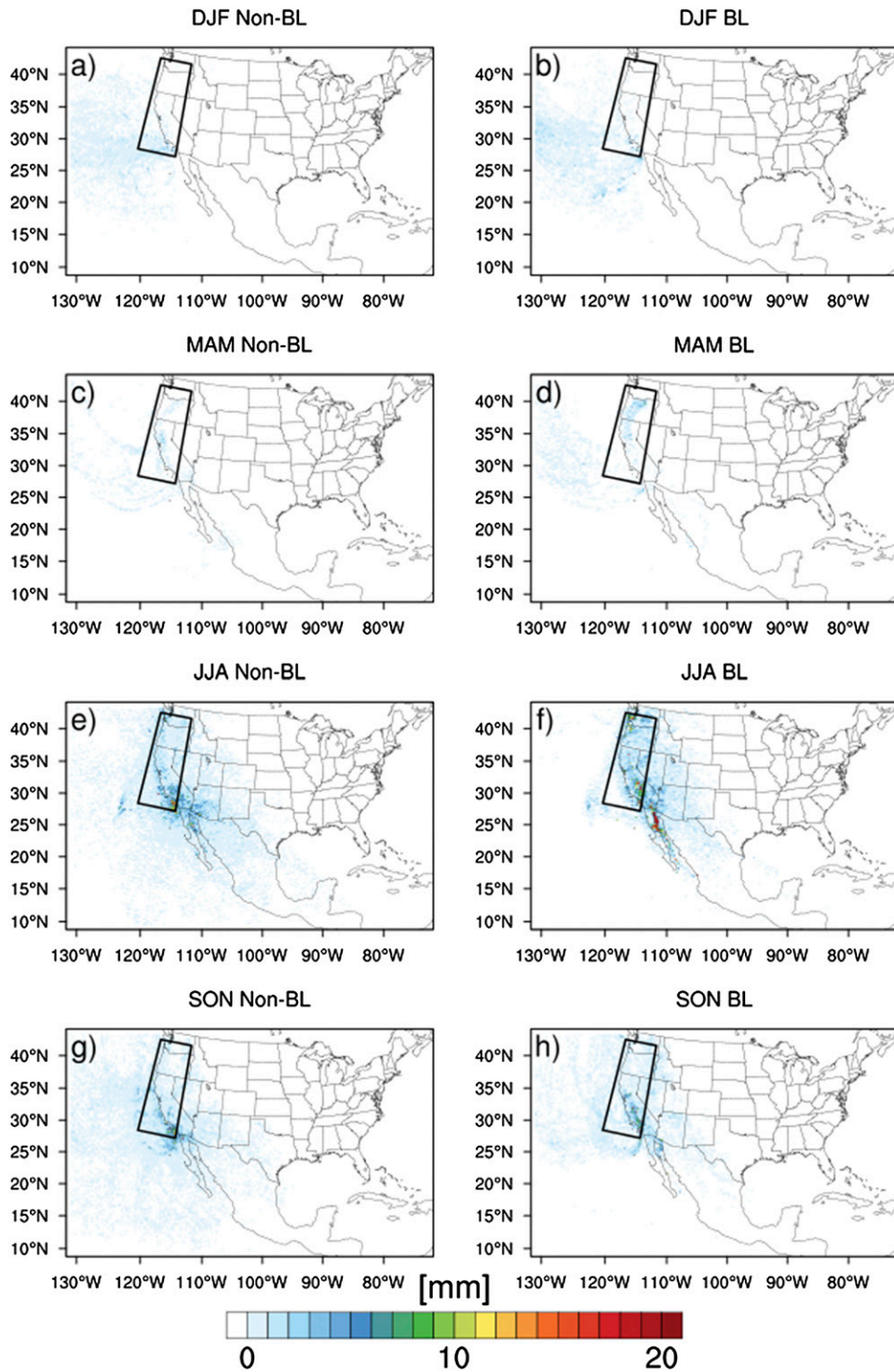


FIG. 2. Total boundary layer uptakes and nonboundary layer uptakes (mm) by season for Region 1 (West Coast).

Region 2

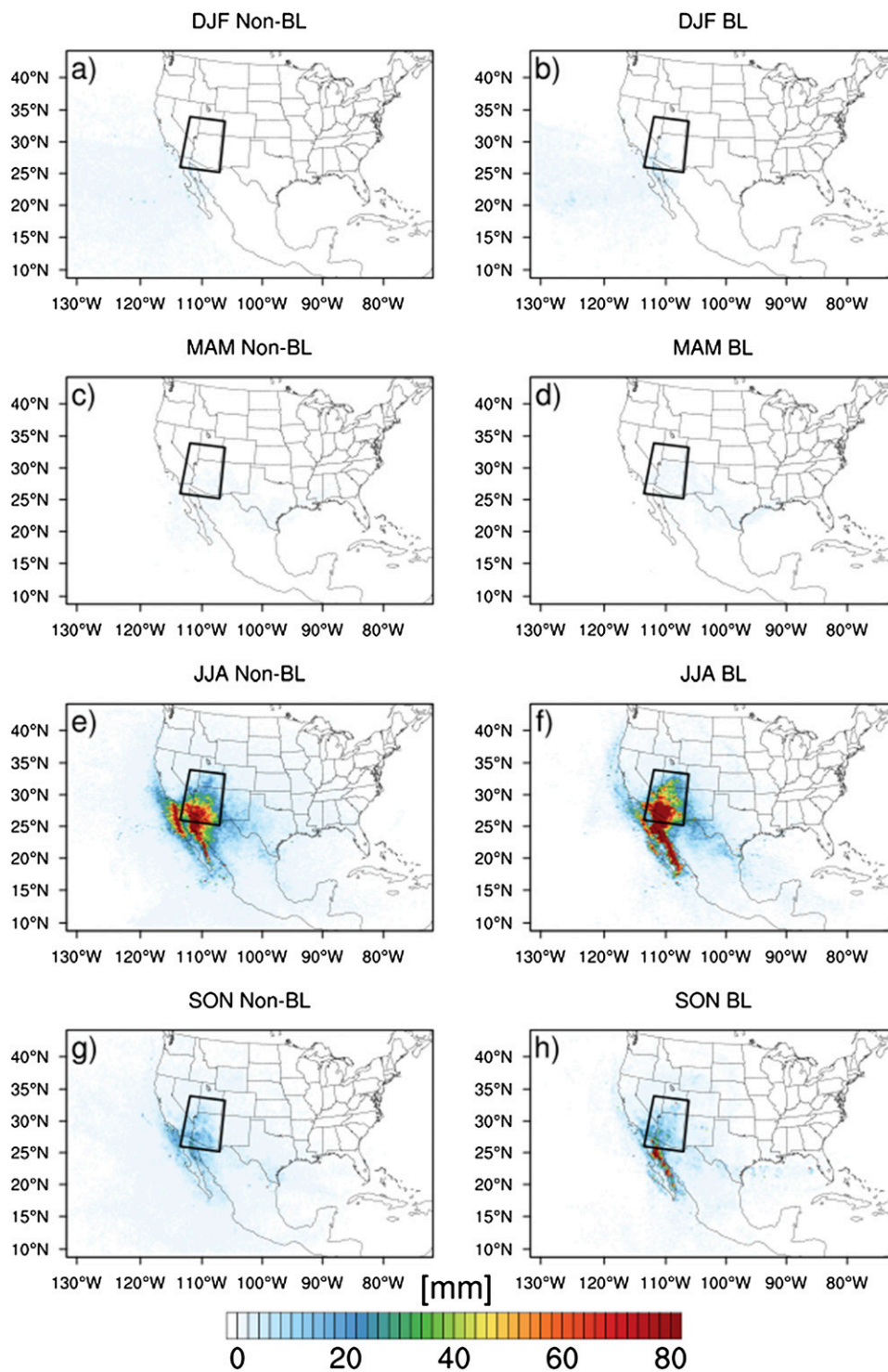


FIG. 3. As in Fig. 2, but for Region 2 (Arizona).

Region 3

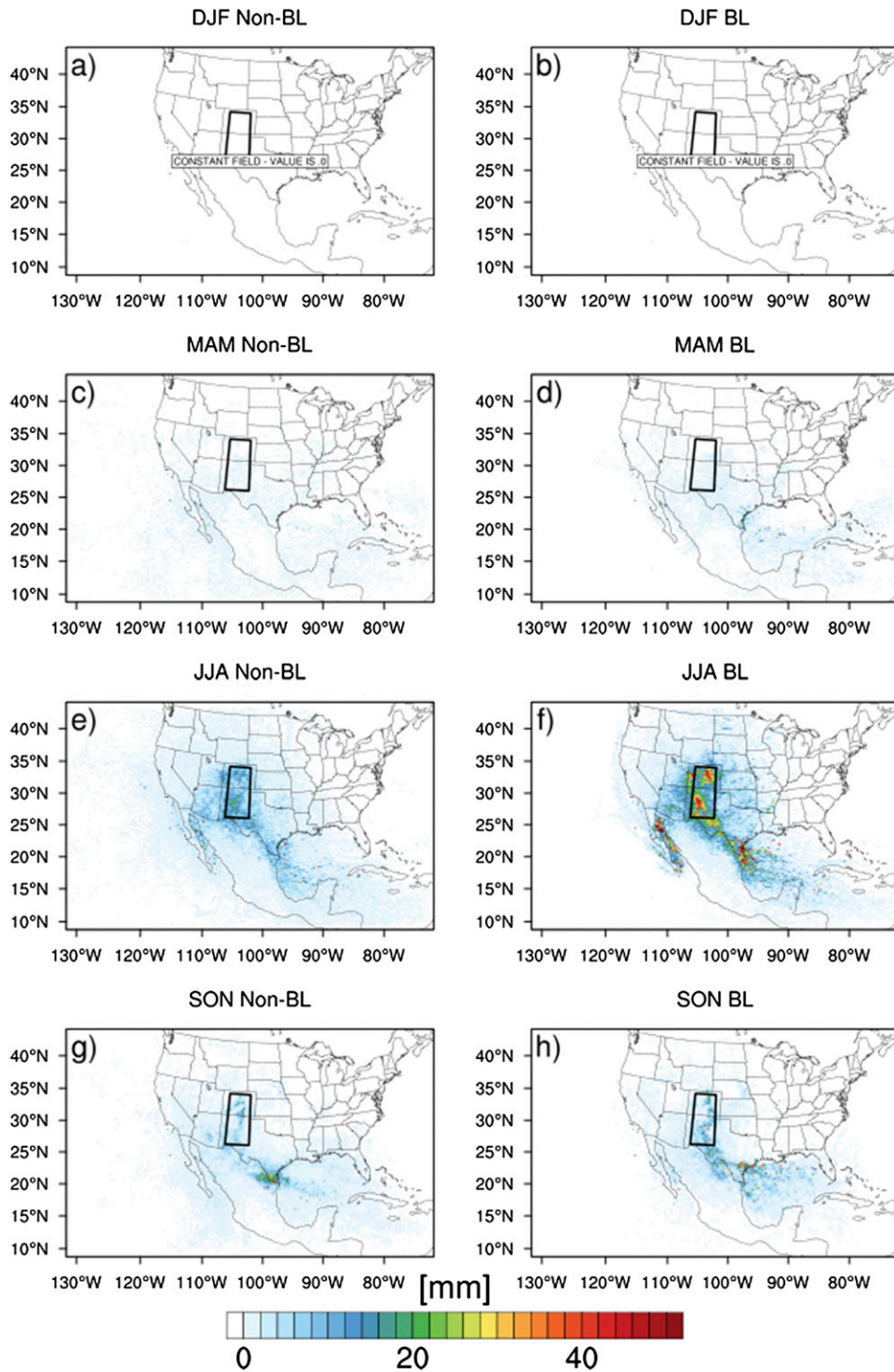


FIG. 4. As in Fig. 2, but for Region 3 (Front Range).

Region 4

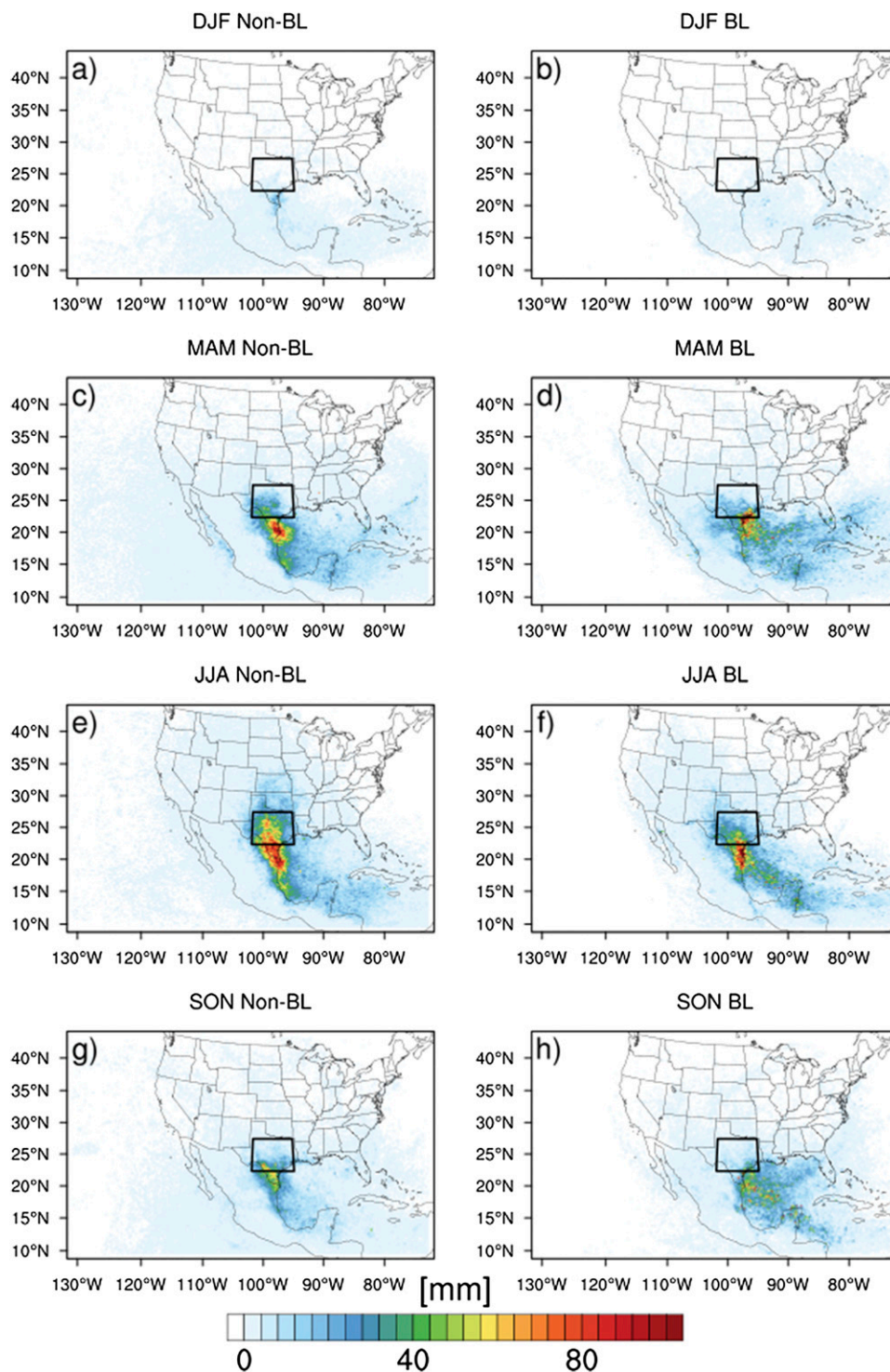


FIG. 5. As in Fig. 2, but for Region 4 (Flash Flood Alley).

Region 5

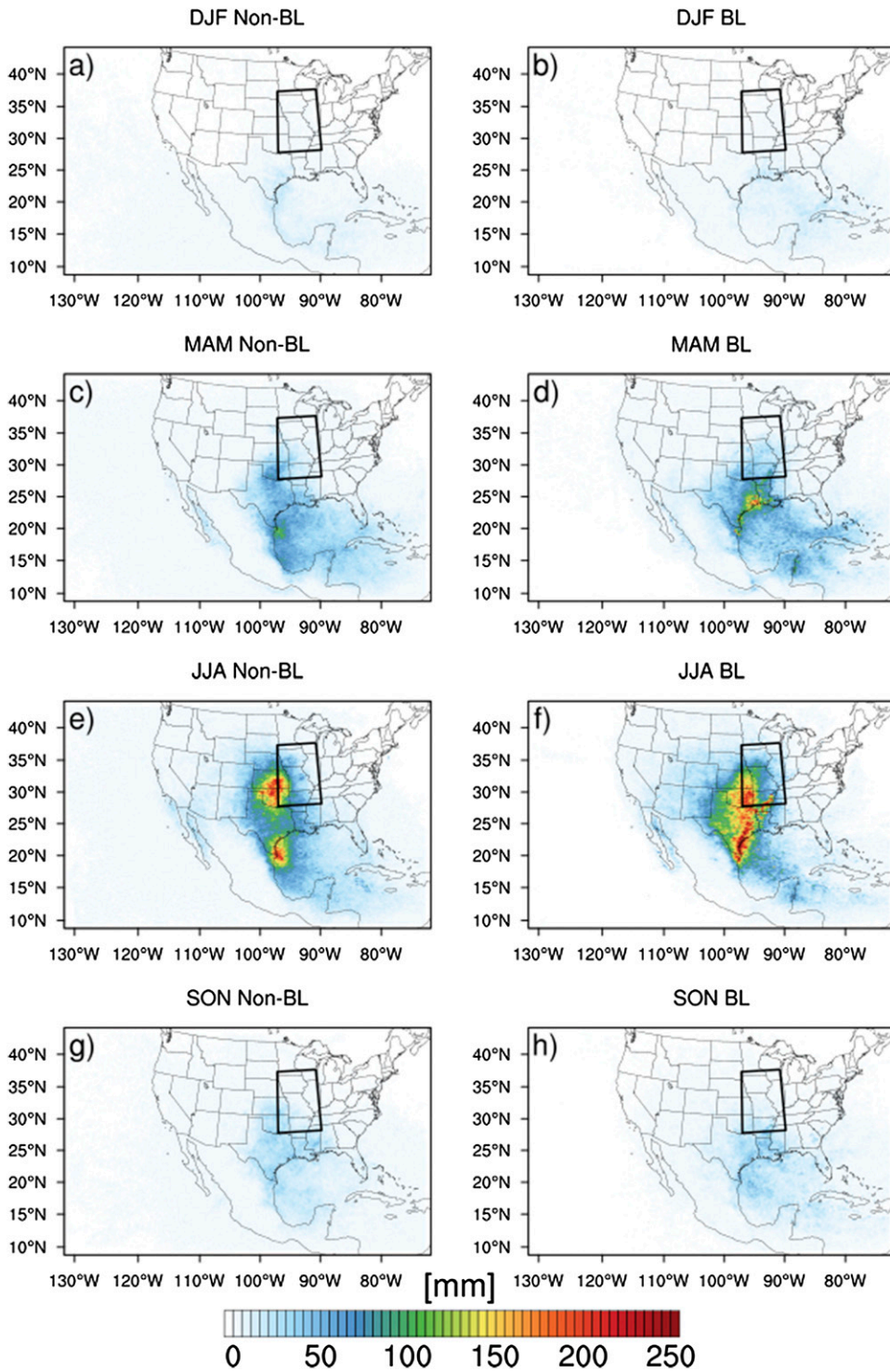


FIG. 6. As in Fig. 2, but for Region 5 (Missouri Valley).

Region 6

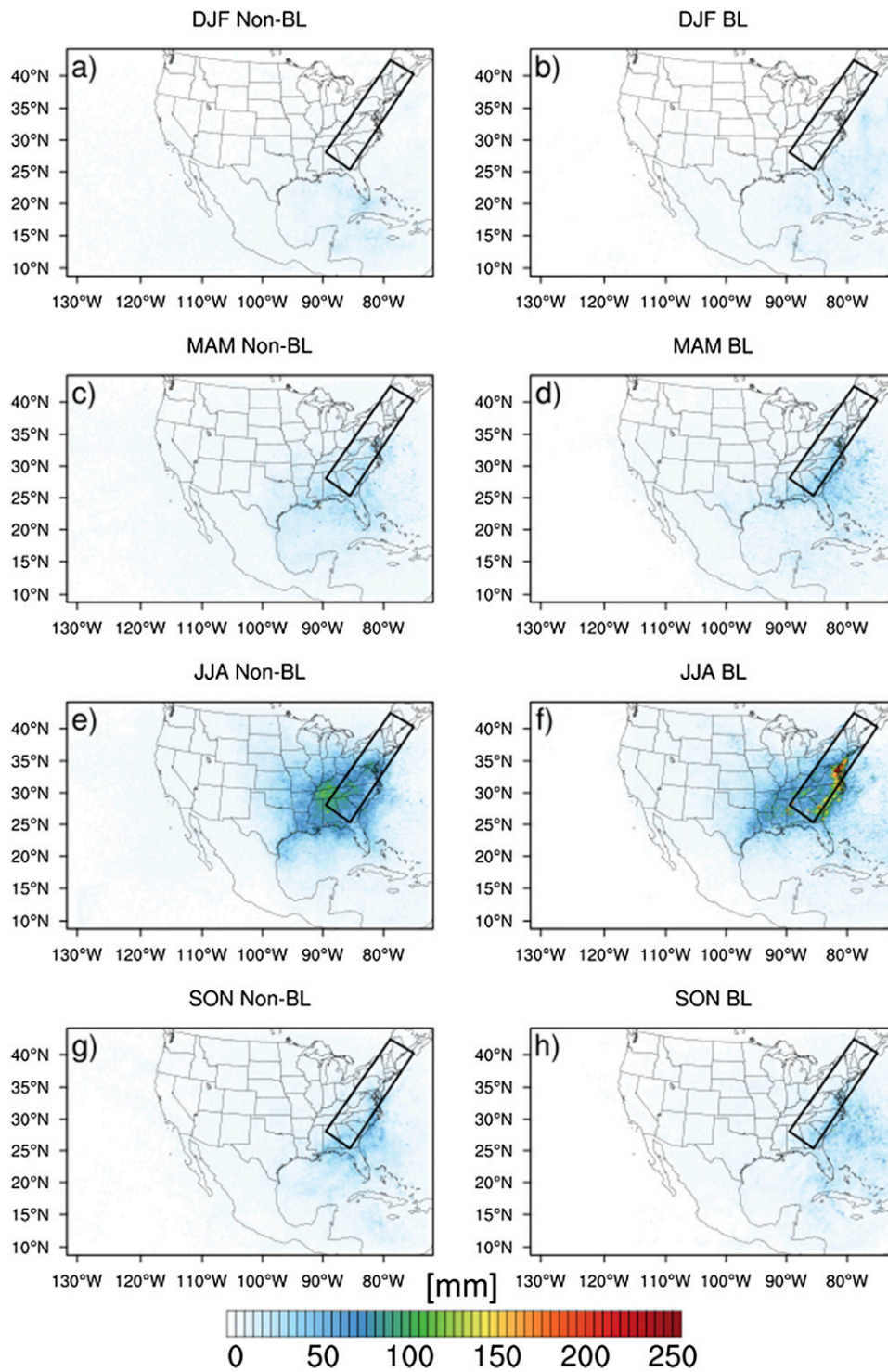


FIG. 7. As in Fig. 2, but for Region 6 (Appalachians).

TABLE 1. Median values (from all trajectories in the specified region and season) of contributions to the final specific humidity of the parcel from boundary layer uptakes (BL), nonboundary layer uptakes (Non-BL), and the residual amount (Other), which is a combination of the initial moisture, advection, and uptakes less than 0.1 g kg^{-1} . For each parcel, these values sum to 1.0, though the median values may not.

	DJF			MAM			JJA			SON		
	BL	Non-BL	Other									
Region 1	0.13	0.00	0.85	0.41	0.00	0.51	0.36	0.06	0.48	0.27	0.09	0.53
Region 2	0.26	0.06	0.56	0.57	0.09	0.32	0.44	0.11	0.40	0.38	0.07	0.48
Region 3	—	—	—	0.50	0.07	0.36	0.45	0.04	0.43	0.36	0.06	0.51
Region 4	0.35	0.12	0.29	0.45	0.12	0.32	0.38	0.17	0.40	0.48	0.10	0.34
Region 5	0.48	0.14	0.28	0.47	0.15	0.29	0.44	0.13	0.37	0.42	0.11	0.41
Region 6	0.50	0.10	0.27	0.47	0.10	0.32	0.43	0.06	0.44	0.63	0.12	0.72

uptakes over Texas and Oklahoma. Nonboundary layer sources of moisture can be attributed to precipitation evaporating into a column or vertical transport of moisture by convection.

For Region 6 (Appalachian Mountains), boundary layer uptakes occur in the Atlantic Ocean and along the coastal plains in Georgia, the Carolinas, and Virginia (Fig. 7). In JJA, the maximum uptakes occur in the coastal regions of the states and farther north into the Chesapeake Bay. In JJA, this is also accompanied by a large, weaker area of boundary layer moisture increases in the Southeast, from eastern Arkansas, to the Gulf of Mexico, through Tennessee, Kentucky, and West Virginia. In the fall, the Atlantic Ocean and coastal regions along the eastern seaboard become the primary source regions for boundary layer uptakes of moisture. In JJA for Region 6, the maximum source for nonboundary layer moisture is over central Tennessee. In this case, there is not a maximum in moisture uptakes along the coast. In MAM and SON, there is a broad region of lower moisture increases in the Southeast and along the Gulf Stream.

b. Relative importance of moisture uptake locations and sources

A summary of the median relative contributions from boundary layer and nonboundary layer uptakes for each region and season is presented in Table 1. For each parcel, the relative contributions of the three categories sum to 1, but the median values of the distribution for each region and season may not meet that criterion. Partitioning the relative contributions for each region and season allow us to quantify the relative importance of each moisture source to floods at that location. The third category (Other) represents the collective contributions to specific humidity from the parcel's initial moisture (advection) and small uptakes less than 0.1 g kg^{-1} , plus any other effects due to the limitations of the methodology discussed above.

For Region 1 (West Coast) during DJF, where the primary driver of cool season heavy rainfall and flash

flooding involves moisture transport across the Pacific Ocean, and the effect of extratropical cyclones, the median values for the fraction of parcel water vapor content that is advected/other is 0.85, that is 50% of parcels have more than 85% of their ending water vapor attributed to advection. In other seasons, the median fraction of advected water vapor is approximately 50% (0.51 in MAM, 0.48 in JJA, and 0.53 in SON).

In Region 2 (Arizona), a similar pattern of advection dominates events occurring in DJF, with 50% of parcels having 56% or more of their water vapor prior to the start of the 120-h trajectories. As with Region 1, the fractions of boundary layer contribution and advective contribution were most equal during JJA and SON during the North American monsoon (NAMS). MAM events saw 50% of parcels have 57% or greater contribution from the boundary layer. Nonboundary layer uptakes were maximized in JJA, though these uptakes remained a small amount of the final specific humidity of parcels.

Along the Front Range (Region 3), the advective contribution to the parcels' final specific humidity is largest in SON, followed closely by JJA. In JJA, as in the previous regions, the distributions of fractional contributions of boundary layer moisture and the advective component are similar. In SON, there is a larger advective component, and in MAM there is a larger fractional contribution of boundary layer moisture. In all cases, the nonboundary layer contribution to parcel specific humidity has a median value less than or equal to 7%.

In Flash Flood Alley (Region 4), cool season advection is no longer the largest constituent of parcel specific humidity. In this case the median value of the fractional contribution of boundary layer moisture is 35%, whereas for advection it is 29%. In MAM, boundary layer uptakes represent the largest source of parcels' moisture (45%), whereas advection/other and boundary layer uptakes are relatively balanced in summer. Boundary layer moisture again represents the largest median contribution in fall.

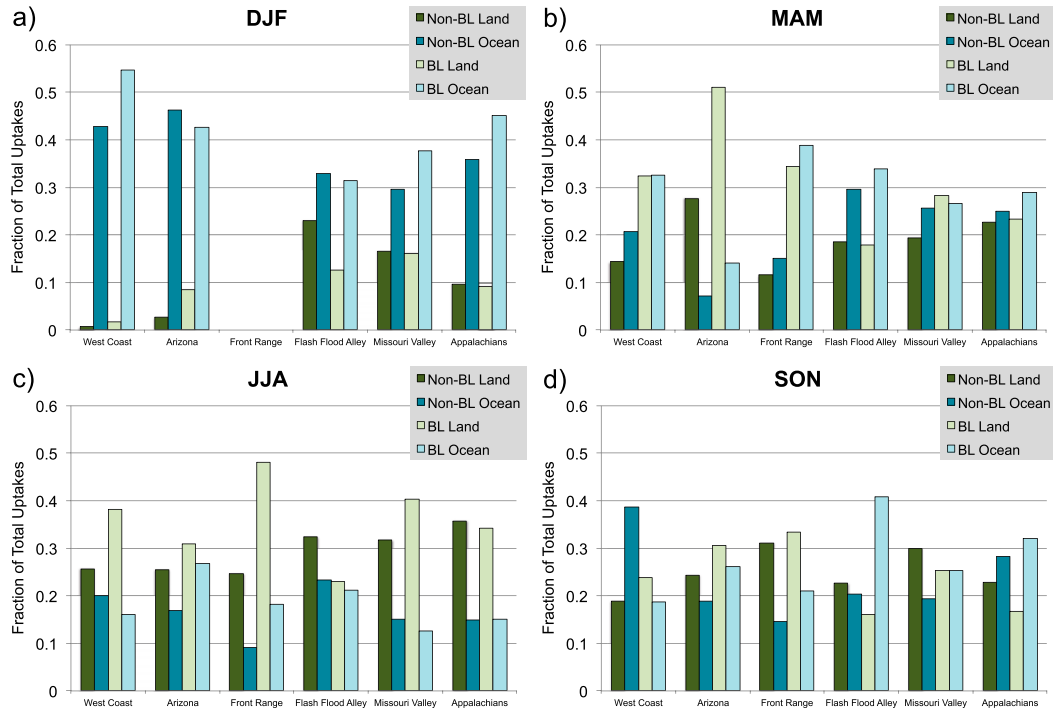


FIG. 8. Relative contributions for nonboundary layer uptakes over land, nonboundary layer uptakes over ocean, boundary layer uptakes over land, and boundary layer uptakes over ocean for (a) DJF, (b) MAM, (c) JJA, and (d) SON.

For Region 5 (Missouri Valley), the rightmost tails of the distributions are populated by contributions from the boundary layer in DJF and MAM, with median values of 48% and 47%, respectively. In summer and fall, these contributions are more balanced. As with all other regions, the nonboundary layer contribution is smallest. In the Appalachians (Region 6), the fractional contributions of boundary layer moisture are largest during DJF and MAM, with median values of 50% and 47% respectively. In JJA, they are relatively balanced, and in SON, advection dominates.

The integrated versions of Figs. 2–7 are shown in Fig. 8 in order to quantify the relative contributions of each of the following four categories for each region and season: nonboundary layer uptakes over land, boundary layer uptakes over land, nonboundary layer uptakes over ocean, and boundary layer uptakes over ocean. In this analysis, the advection/other component discussed earlier in this section is neglected, and we consider only increases along the parcel trajectory. For each season and region, the four categories will sum to 1. The importance of oceanic sources of moisture is highlighted in the cool season for all regions, while the moisture sources over land are most important for warm season floods. Land surface moisture plays a negligible role for cool season flash flooding in Region 1, whereas flash flooding during the NAMS in Region 2 during the warm

season shows nearly equal uptakes from oceanic and land surface source in both the boundary layer and above it. Region 3 is influenced more heavily by land surface moisture contributions during their climatologically favored seasons of flash flooding in JJA and SON. Region 4 has nearly equal contributions from oceanic and land surface sources during JJA, but the boundary layer ocean category dominates in SON presumably due to tropical cyclones. Region 5 reveals stronger atmosphere–land surface coupling with terrestrial moisture sources being equal to oceanic ones in MAM but becoming more significant in SON and especially JJA. The relative contributions to flash flooding in Region 6 are similar to those in Region 5 with an increase of the oceanic contribution in SON, likely a result from tropical cyclones as in Region 4.

c. Surface properties at boundary layer uptake locations

Climatologies of sensible and latent heat fluxes were generated from the HRLDAS simulation at 3-hourly intervals for each month. For example, a latent heat flux climatology for 1800 UTC in June would contain mean values at 1800 UTC from all 1800 UTC hours in the month of June from 2007 to 2013. Over the oceans, flux climatologies were calculated from NARR data instead of HRLDAS data, given HRLDAS does not simulate the oceans.

Region 1 JJA

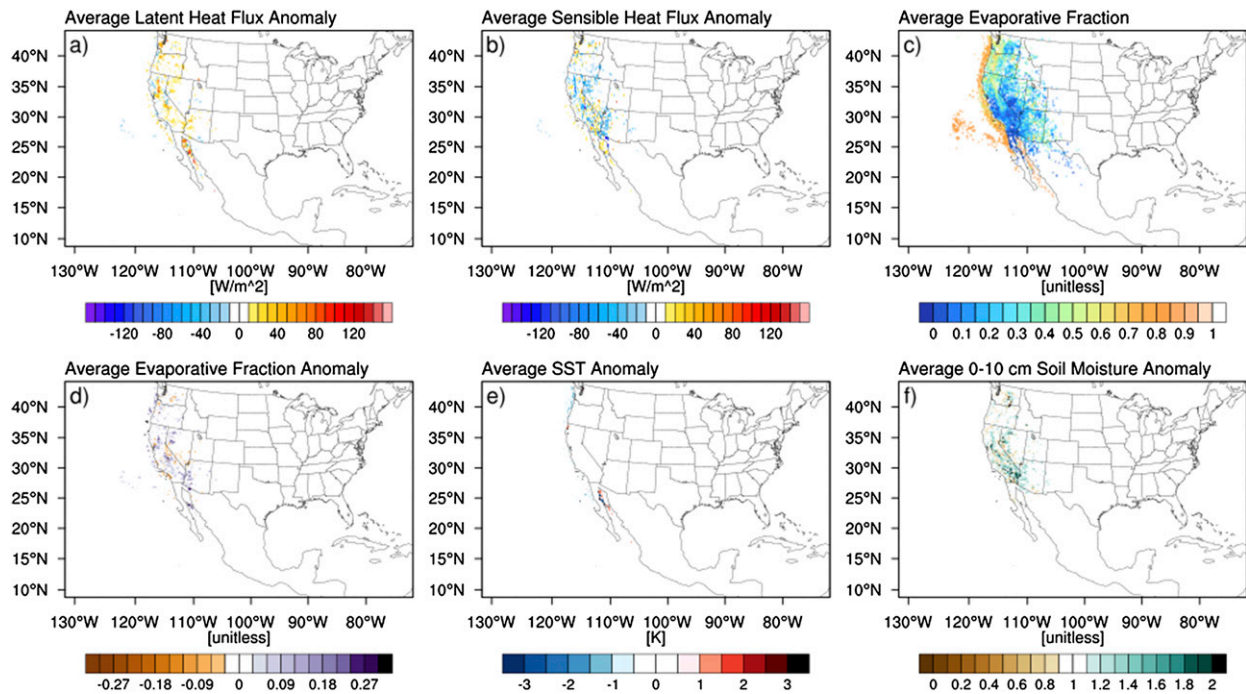


FIG. 9. Average (a) latent heat flux anomalies (W m^{-2}), (b) sensible heat flux anomalies (W m^{-2}), (c) evaporative fraction, (d) evaporative fraction anomalies, (e) SST anomalies, and (f) top-layer (0–10 cm below ground) soil moisture anomalies (as ratio of normal) for boundary layer uptakes for the West Coast (Region 1) in JJA.

The along-trajectory sensible and latent heat flux anomalies were calculated by comparing the values associated with flash floods to the climatological values. In these cases, pixels with five events or more are retained to reduce noise in the data. (Including all pixels leads to extrema when only one data point is present for a grid cell.) The data at uptake points were also analyzed in terms of evaporative fraction, defined as the ratio of latent heat to the available energy of the land surface:

$$EF = \frac{LH}{LH + SH}. \quad (11)$$

The evaporative fraction yields how available energy at the surface is partitioned, and values that approach 1 indicate that available energy is used for evaporation, whereas evaporative fractions that approach 0 indicate that available energy is transferred from the surface to the atmosphere as heat. Additionally, anomalies in evaporative fraction (computed as departures from the evaporative fraction climatology computed from latent and sensible heat fluxes at each hour for each month) were examined at each point a boundary layer uptake occurred. Concurrently analyzing anomalies in surface fluxes along with how they are partitioned (evaporative

fraction) describes the state of the land surface more fully. For example, if surface latent heat fluxes are anomalously large and surface sensible heat fluxes are also anomalously large, the anomaly may be due to increased radiative forcing (e.g., a clear, sunny day in an area where it is usually cloudy in the climatology), which does not affect the partitioning of the available energy at the land surface. If surface latent heat fluxes are anomalously large and sensible heat fluxes are anomalously low at a point, then the evaporative fraction also contains a positive anomaly, and this is a case of increased surface evaporation.

In a similar fashion, sea surface temperature (SST) anomalies were computed relative to the NARR long-term average (1979–2008 monthly mean) at each point a boundary layer uptake occurred. The following figures summarize the character of the land surface at the location of boundary layer uptakes. Locations with five or more uptakes are plotted to reduce artificial extrema that occurred when fewer than five points were averaged. Anomalies of fluxes, evaporative fraction, and SST are computed as departures from normal.

For the West Coast, there are slight positive latent heat flux anomalies in central California, over the Gulf of California, and in Nevada in JJA (Fig. 9, median

Region 2 JJA

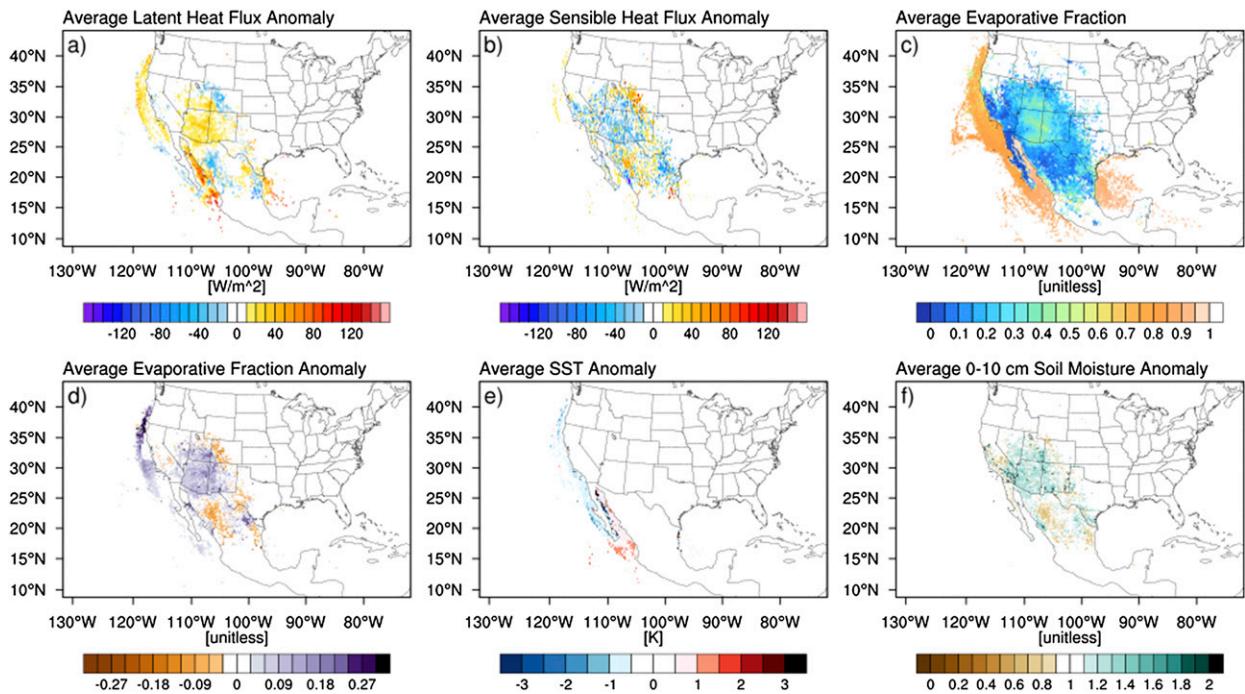


FIG. 10. As in Fig. 9, but for Region 2 (Arizona) during JJA.

domain positive anomaly of 11.81 W m^{-2}) and SON (Fig. S3, median domain positive anomaly of 37.32 W m^{-2}), respectively. (Note that, while certain regions and seasons of interest are highlighted in this section, figures for all regions and seasons can be found in the supplemental material included with this manuscript.) These areas correspond with slight negative sensible heat flux anomalies [median domain negative anomaly of -15.96 W m^{-2} (JJA) and -11.82 W m^{-2} (SON)]. This indicates that, within the confines of this study domain, the moisture for flash floods on the West Coast is transported with little modification by the land surface.

For the monsoonal region (Region 2), positive latent heat flux anomalies occur in the Gulf of California in JJA (Fig. 10). In SON (Fig. S6), these anomalies occur over the Southwest as well as over the Gulf of California. Sensible heat fluxes are anomalously low over the Southwest during these two seasons except over the Gulf of California. These anomalous fluxes are spatially correlated with warm SSTs ($>0.5 \text{ K}$ above average) in the Gulf of California in JJA. Over the Southwest, evaporative fractions range generally from 0.2 to 0.5, whereas over the water, they approach 1.0. However, over the Gulf of California, the fluxes are not anomalously partitioned, but there are slight positive anomalies in evaporative fraction over the Southwest in JJA, and larger evaporative fraction anomalies in Arizona,

Southern California, southern Nevada, and southern Utah. Soil moisture is anomalously high over the same region contributing to larger than normal surface evaporation and latent heat fluxes, indicative of local recycling.

Flash floods occurring along the Front Range (Region 3) have a climatological maximum in JJA (Fig. 11). Slight positive anomalies in surface latent heat fluxes where boundary layer uptakes occur are present over much of the SGP and Southwest as well as portions of the western Gulf of Mexico and Gulf of California. These anomalies are largest in central Texas, eastern Oklahoma and central Kansas, where they are also accompanied by negative anomalies in surface sensible heat fluxes. Over Oklahoma and Kansas, evaporative fractions exceed 0.6. The partitioning of surface fluxes is also anomalous, with positive anomalies in evaporative fraction occurring over this region as well. Positive SSTs are present in the Gulf of California for JJA. The combination of anomalous latent heat fluxes and higher than normal SSTs in the Gulf of California indicate that some summer floods along the Front Range have similar signatures in land–atmosphere interactions as the North American monsoon, whose patterns of surface flux and SST anomalies were discussed for the previous region. The land areas with the largest latent heat flux anomalies also contain large top-layer soil moisture

Region 3 JJA

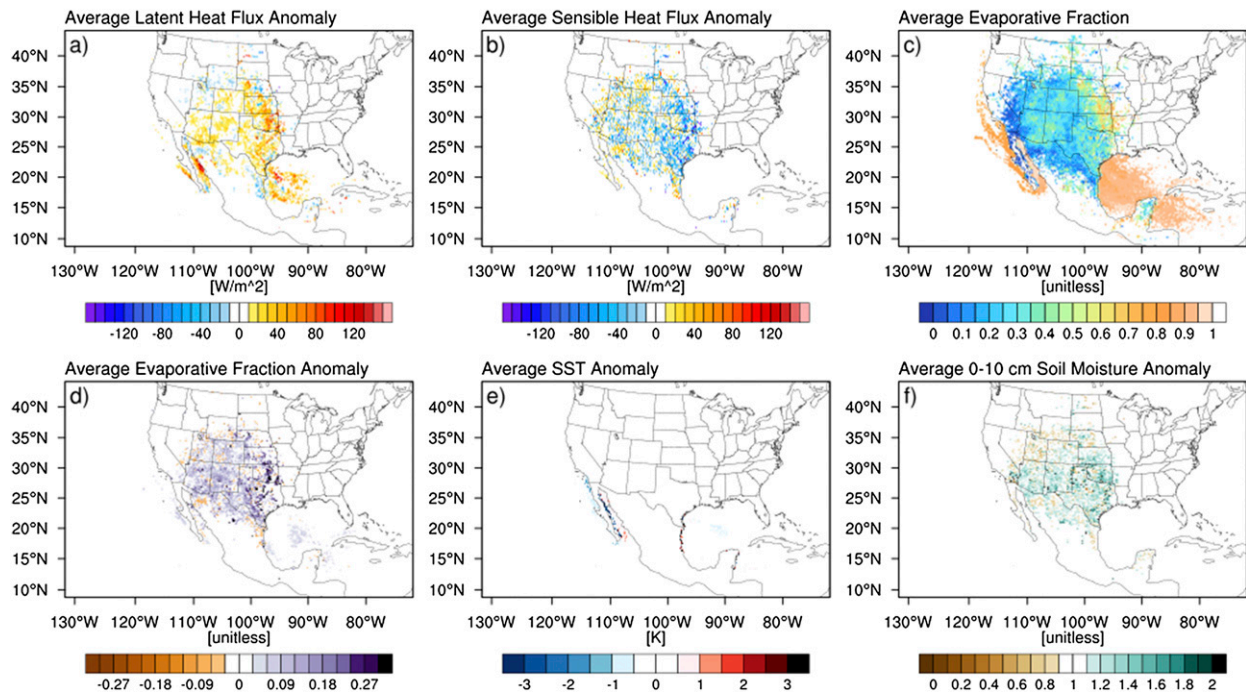


FIG. 11. As in Fig. 9, but for Region 3 (Front Range) during JJA.

anomalies ($>150\%$ of normal). Additionally the low-level flow indicated a western branch for some events that passes over the Gulf of California. Positive SSTs also occurred off the Texas coast for flash floods occurring in SON for the Front Range (Fig. S8). An arc of collocated large positive latent heat flux anomalies, negative sensible heat flux anomalies, positive evaporative fraction anomalies, and positive soil moisture was present along the flow pattern over northern Mexico, through New Mexico, and into eastern Colorado.

In Flash Flood Alley (Region 4), most flash floods occur in MAM (Fig. S10) and JJA (Fig. 12). For boundary layer uptakes for floods occurring in MAM, there are very large latent heat flux anomalies in the northern Gulf of Mexico (median domain positive anomaly of 54.68 W m^{-2} over water), accompanied by slight positive anomalies in sensible heat flux (median domain positive anomaly of 8.51 W m^{-2} over water). Over land, there are large positive latent heat flux anomalies over most of Texas (median domain positive anomaly of 13.02 W m^{-2} , though larger over Texas), collocated with negative sensible heat flux anomalies (median domain negative anomaly of -25.67 W m^{-2}). With evaporative fraction values greater than 0.5 in magnitude, this also results in a positive evaporative fraction anomaly. SST anomalies are neutral in the Gulf of Mexico, but positive top-layer soil moisture anomalies accompany the

anomalies in latent heat fluxes, signifying that anomalous evaporation is occurring from wet soils in Texas.

During JJA, there is a large swath of positive latent heat flux anomalies over the Gulf of Mexico (median domain positive anomaly of 37.15 W m^{-2} over water), but this axis has shifted south and west, reflecting the prevalent flow pattern. These are accompanied by mostly neutral sensible heat flux anomalies (median positive anomalies of 1.85 W m^{-2} and negative anomalies of -2.34 W m^{-2}). Over land, however, there are strongly negative sensible heat flux anomalies (median negative anomaly of -42.03 W m^{-2}) that are collocated with large positive latent heat flux anomalies over the Balcones Escarpment specifically. Here, evaporative fraction values are above 0.6 and are highly positively anomalous. Additionally, there are positive anomalies in SSTs in the central Gulf of Mexico and Caribbean Sea in JJA as well as positive soil moisture anomalies over Mexico, New Mexico, and Texas.

During SON, there are positive latent heat flux anomalies for boundary layer uptakes occurring over the Gulf of Mexico, as well as positive sensible heat flux anomalies and warm SST anomalies throughout the Gulf of Mexico (Fig. S11). Over land, the anomalies in surface fluxes are less widespread than in MAM and JJA, but there still remain some positive latent heat flux anomalies, negative sensible heat flux anomalies,

Region 4 JJA

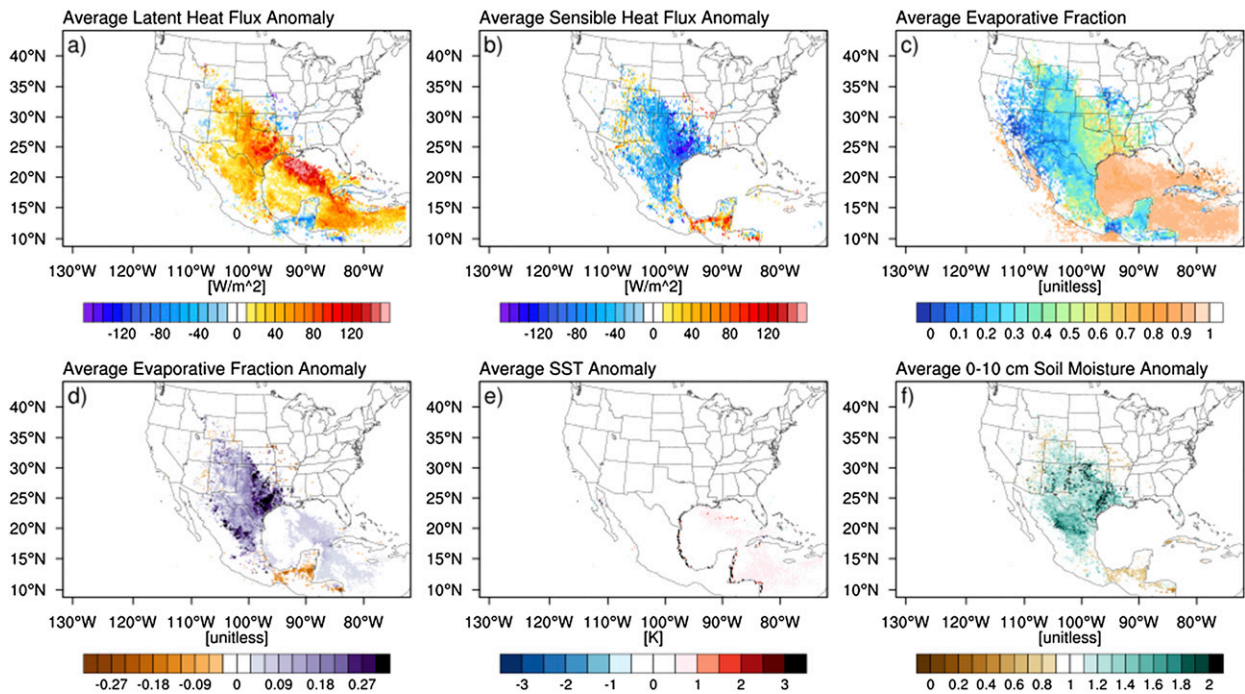


FIG. 12. As in Fig. 9, but for Region 4 (Flash Flood Alley) during JJA.

and positive evaporative fraction anomalies over central Texas.

Flash floods during the warm season in the Missouri Valley (Region 5) are characterized by anomalies in surface fluxes and the largest average evaporative fractions over land in large areas of the contiguous United States (CONUS). For boundary layer uptakes for floods occurring in MAM, the largest latent heat fluxes occur in the Gulf of Mexico and Atlantic Ocean off the Florida coasts (Fig. 13). Over land, there are positive latent heat flux anomalies over Texas, Oklahoma, Kansas, Missouri, Arkansas, and Missouri, all of which are accompanied by negative sensible heat flux anomalies, and positive anomalies in evaporative fraction. There are slight positive anomalies in SST along the flow south of Florida and generally neutral top-layer soil moisture anomalies over the CONUS. Positive sensible heat flux anomalies occurring over the Atlantic Ocean and Gulf of Mexico as well as in smaller areas over Kentucky, Tennessee, and Ohio could contribute to enhanced instability of parcels originating near the surface.

During summer (JJA), latent heat flux anomalies for boundary layer uptakes persist in the Gulf of Mexico off the coasts of Florida and Alabama and in the Caribbean Sea (Fig. S13). The maximum in latent heat flux positive anomalies, however, shifts northward, and is centered

over Nebraska, Iowa, eastern Kansas, and western Missouri. Again, these positive anomalies are collocated with negative anomalies in sensible heat fluxes, resulting in positive evaporative fraction anomalies. Over Iowa, Missouri, Illinois, and eastern Kansas, evaporative fractions exceed 0.6, indicating that most of the available energy at the surface is used for evaporation. Additionally, there are slight positive anomalies in soil moisture, but these are not as anomalous as those that occurred in western regions.

During SON, positive latent heat flux anomalies are present in the northern Gulf of Mexico, off the coasts of the Carolinas, and in the Caribbean Sea (Fig. S14). In the case of the Atlantic Ocean, these are also regions of abnormally high latent heat fluxes and SSTs. The maximum in latent heat fluxes over land shifts southward to Missouri, Kansas, Oklahoma, and Arkansas, and this is a region of negative anomalies in surface sensible heat fluxes and positive anomalies in evaporative fraction. Additionally, in Missouri, there are positive top-layer soil moisture anomalies.

Floods occurring along the Appalachians (Region 6) are associated with anomalously high latent heat fluxes in the Northeast and in the Atlantic during MAM (Fig. S16). Over land, these regions are also associated with negative sensible heat flux anomalies and positive anomalies in evaporative fraction. Positive anomalies in

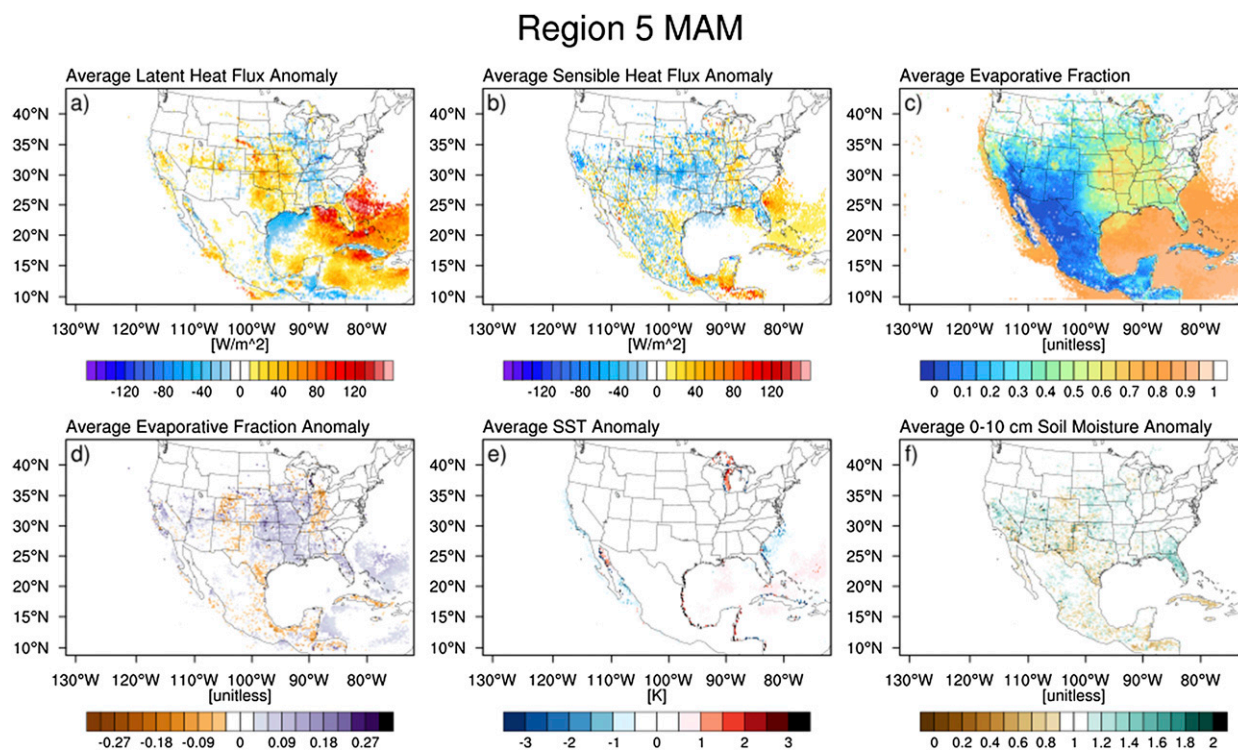


FIG. 13. As in Fig. 9, but for the Missouri Valley (Region 5) during MAM.

SST occur along the East Coast, but average top-layer soil moisture anomalies are neutral in MAM. During summer (Fig. S17), there are again positive latent heat flux anomalies in the Atlantic Ocean and Gulf of Mexico, the largest of which are collocated with slight sensible heat flux anomalies and warmer than average SSTs. Great Lakes temperatures are also warmer than average. Large values of evaporative fraction are present in Kentucky and Tennessee and northeastward through New England, and there are slight positive anomalies nearly everywhere east of the Mississippi, though soil moisture anomalies are neutral.

In SON, there are positive SST anomalies in the Gulf of Mexico in addition to those off the East Coast, collocated with areas of highly anomalous latent and sensible heat fluxes (Fig. 14). Given that tropical cyclones (or extratropical cyclones that had their start as tropical cyclones) are a key driver of flooding in this region, it is unsurprising to see warm SSTs in the Gulf of Mexico during hurricane season in the Atlantic basin. The positive anomalies in sensible heat fluxes would also increase the instability of surface-based parcels in these regions. Over land, large latent heat fluxes and low sensible heat fluxes lead to evaporative fraction anomalies in the mid-Atlantic, though the pattern is reversed over Iowa and Illinois. Again, for this region, top-layer soil moisture is not especially anomalous, though there

are positive anomalies along the East Coast, and slight dry anomalies in Iowa, Illinois, and Missouri.

4. Summary and conclusions

The centroids of 19 253 flash flood reports from NWS *Storm Data* during the period 2007–13 were used to initialize backward trajectories to study source regions for flash flood events. Parcels were distributed horizontally in $66 \text{ km} \times 66 \text{ km}$ grids with 30 hPa spacing in the vertical (from 950 to 470 hPa). Parcels were launched from these three-dimensional boxes, centered on the flash flood report, and traced backward 120 h (5 days) to 1) assess the dominant track of parcels that terminate at mandatory pressure levels in flash flooding setups; 2) identify regions where parcels increased their specific humidity; 3) determine whether or not those moisture uptakes occurred within the boundary layer, having some influence from the land surface properties; and 4) characterize the properties of the land surface when parcel moisture uptakes were linked to the boundary layer. This work extends the methodology described in Sodemann et al. (2008) by including the land surface properties from a multiyear HRLDAS simulation, the offline version of the Noah land surface model, where boundary layer uptakes were observed.

Region 6 SON

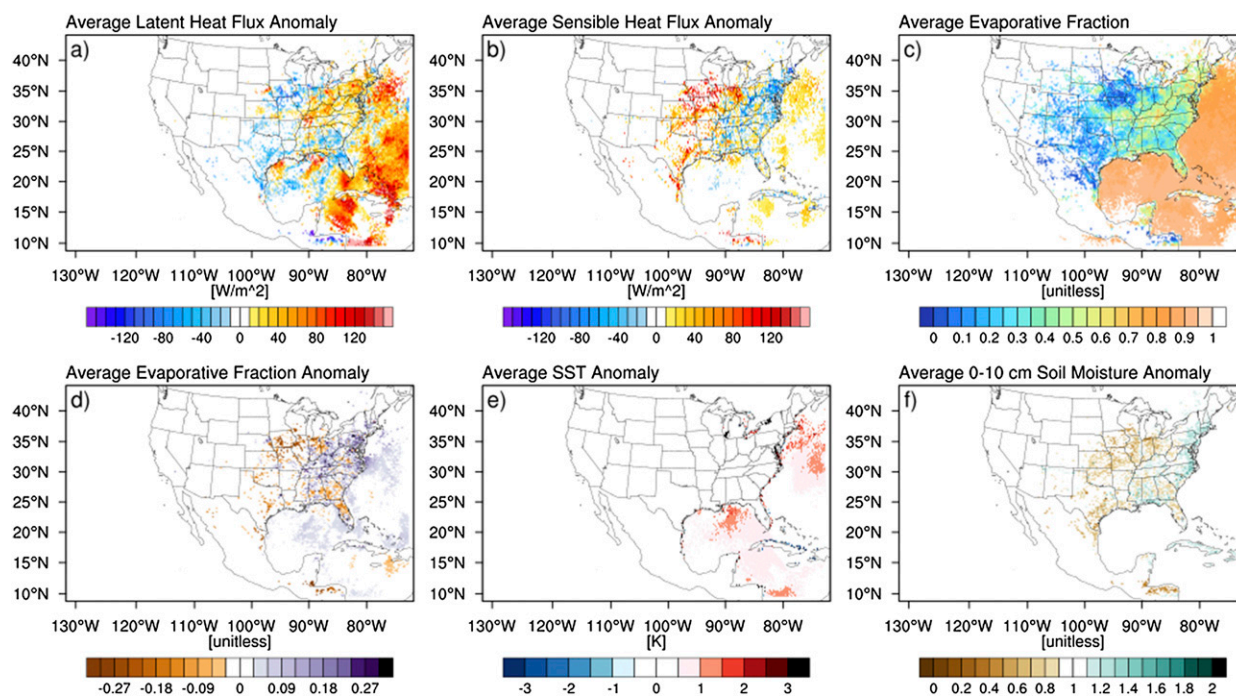


FIG. 14. As in Fig. 9, but for the Appalachians (Region 6) during SON.

The analysis was divided into six regions of interest: 1) West Coast, 2) Arizona, 3) Front Range, 4) Flash Flood Alley, 5) Missouri Valley, and 6) Appalachians according to the flashiness regions delineated by Saharia et al. (2017). Cases were subdivided further by season (DJF, MAM, JJA, and SON) in order to study the seasonality of flash flood mechanisms. This methodology, though uniquely applied here to the flash flood problem, elucidates that many well-known climatological mechanisms are key components for heavy rainfall in these regions. The land surface was found to have a positive contribution to the moisture budget for flash flood events for the United States, though the extent to which this is true varies regionally and seasonally.

The predominant source regions of boundary layer moisture for flash floods in the United States are the Gulf of Mexico and the Gulf of California. The Gulf of California is most influential during JJA and SON, when the North American monsoon is active. The Gulf of Mexico is a key source of moisture for flash floods occurring east of the Continental Divide for all seasons. Most of the mass that is evaporated from these bodies of water occurs over the summer months, which is the peak season for flash flooding in the CONUS. During the cool season, however, the relative contributions of the ocean are much larger than those over the land, even though

the total mass contributed for flash flood events is smaller than in the warm season.

The terrestrial area where most of the boundary layer uptakes occur is the south-central United States, which includes the southern Great Plains, a known hotspot for land–atmosphere interactions. The contribution of land surface plays the largest relative role in the warm season (JJA) across all regions. In the spring and fall, the results vary by region. From a vertical perspective, all regions exhibit nearly unidirectional or slightly veering flow with height throughout a deep layer in the lower troposphere.

Sources of nonboundary layer moisture could be due to a combination of sources which are unaccountable using this methodology: precipitation evaporated into the column, vertical transport by convection or advection, or advection laterally from regions other than along the track of the trajectory. Further research should include a lagged release of parcels along the trajectory to address the latter effect, but that is beyond the scope of the present study. Nonboundary layer sources of moisture tend to coincide with boundary layer sources of moisture over land, though these uptakes are generally lesser in magnitude. Over water, the spatial pattern of where boundary layer uptakes occur versus where nonboundary layer uptakes occur differs, and boundary layer uptakes account for most of the mass taken up over water.

In all regions and seasons, pixels where boundary layer uptakes occur are characterized by anomalously high latent heat fluxes, anomalously low sensible heat fluxes, anomalously large evaporative fractions, and anomalously wet soils in the 0–10-cm layer below ground.

The regionally specific findings of this work can be summarized as follows:

- Surface–atmosphere interactions play a minimal role in West Coast (Region 1) flash flood events, where the moisture budget is dominated by advection.
- The Gulf of California is a key source of moisture for summer monsoon flooding in Arizona (Region 2), and positive SST anomalies are largest in JJA in the Gulf of California.
- The Front Range (Region 3) receives contributions from both the Gulf of Mexico and the Gulf of California.
- In Flash Flood Alley (Region 4), both boundary layer and nonboundary layer uptakes occur over a fetch spanning south of Cuba and through the Gulf of Mexico, the latter of which exhibits positive SST anomalies for flash flood events. This region is also characterized by the strongest land–atmosphere coupling, evidenced by large evaporative fraction anomalies.
- The Missouri Valley (Region 5) exhibits similar patterns in terrestrial uptakes and positive SSTs to that of Flash Flood Alley.
- SST anomalies are also large in regions and season affected by tropical storms in the Atlantic basin (Region 6).
- Avenues for further research include the investigations into the sources of nonboundary layer uptakes detailed previously in this section. This will explain the physical mechanisms behind the signal of moisture uptakes in the deserts of Arizona during JJA as well as the difference between boundary layer uptakes and nonboundary layer uptakes for other regions.

This study seeks to further the knowledge of land–atmosphere interactions and how these interactions exert their effects on flood-producing storms by assessing the locations and magnitudes of moisture sources for flash flood events in the United States. Considering both local and nonlocal effects of the land surface are an important step in forecasting flash floods, not only for the hydrological response of the land surface, but in assessing potential moisture sources for the production of heavy rainfall. As the forecasting paradigm for flash floods shifts to include direct simulation of the land surface and both surface and subsurface flows, it is important that forecasters consider these effects when producing forecasts for heavy rainfall and flash flooding.

Acknowledgments. The first author has been partially supported for this work by the NSF Graduate Research

Fellowship under Grant No. DGE-1102691. Partial funding for this research was provided by the Disaster Relief Appropriations Act of 2013 (P.L. 113-2), which provided support to the Cooperative Institute for Mesoscale Meteorological Studies at the University of Oklahoma (OU) under Grant NA14OAR4830100 and National Science Foundation grant award ICER1663840. Some of the computing for this project was performed at the OU Supercomputing Center for Education and Research (OSCER) at OU.

REFERENCES

- Arnault, J., R. Knoche, J. Wei, and H. Kunstmann, 2016: Evaporation tagging and atmospheric water budget analysis with WRF: A regional precipitation recycling study for West Africa. *Water Resour. Res.*, **52**, 1544–1567, <https://doi.org/10.1002/2015WR017704>.
- Berg, L. K., L. D. Riihimaki, Y. Qian, H. Yan, and M. Huang, 2015: The low-level jet over the southern Great Plains determined from observations and reanalyses and its impact on moisture transport. *J. Climate*, **28**, 6682–6706, <https://doi.org/10.1175/JCLI-D-14-00719.1>.
- Brubaker, K. L., P. A. Dirmeyer, A. Sudradjat, B. S. Levy, and F. Bernal, 2001: A 36-yr climatological description of the evaporative sources of warm-season precipitation in the Mississippi River basin. *J. Hydrometeor.*, **2**, 537–557, [https://doi.org/10.1175/1525-7541\(2001\)002<0537:AYCDOT>2.0.CO;2](https://doi.org/10.1175/1525-7541(2001)002<0537:AYCDOT>2.0.CO;2).
- Chen, F., and J. Dudhia, 2001: Coupling an advanced land surface–hydrology model with the Penn State–NCAR MM5 modeling system. Part II: Preliminary model validation. *Mon. Wea. Rev.*, **129**, 587–604, [https://doi.org/10.1175/1520-0493\(2001\)129<0587:CAALSH>2.0.CO;2](https://doi.org/10.1175/1520-0493(2001)129<0587:CAALSH>2.0.CO;2).
- , and Coauthors, 2007: Description and evaluation of the characteristics of the NCAR high-resolution land data assimilation system. *J. Appl. Meteor. Climatol.*, **46**, 694–713, <https://doi.org/10.1175/JAM2463.1>.
- Dirmeyer, P. A., and K. L. Brubaker, 1999: Contrasting evaporative moisture sources during the drought of 1988 and the flood of 1993. *J. Geophys. Res.*, **104**, 19 383, <https://doi.org/10.1029/1999JD900222>.
- , and —, 2007: Characterization of the global hydrologic cycle from a back-trajectory analysis of atmospheric water vapor. *J. Hydrometeor.*, **8**, 20–37, <https://doi.org/10.1175/JHM557.1>.
- , and J. L. Kinter, 2010: Floods over the U.S. Midwest: A regional water cycle perspective. *J. Hydrometeor.*, **11**, 1172–1181, <https://doi.org/10.1175/2010JHM1196.1>.
- Dominguez, F., P. Kumar, and E. R. Vivoni, 2008: Precipitation recycling variability and ecoclimatological stability—A study using NARR data. Part II: North American monsoon region. *J. Climate*, **21**, 5187–5203, <https://doi.org/10.1175/2008JCLI1760.1>.
- , G. Miguez-Macho, and H. Hu, 2016: WRF with water vapor tracers: A study of moisture sources for the North American monsoon. *J. Hydrometeor.*, **17**, 1915–1927, <https://doi.org/10.1175/JHM-D-15-0221.1>.
- Drumond, A., R. Nieto, L. Gimeno, and T. Ambrizzi, 2008: A Lagrangian identification of major sources of moisture over central Brazil and La Plata Basin. *J. Geophys. Res.*, **113**, D14128, <https://doi.org/10.1029/2007JD009547>.
- Ek, M. B., and L. Mahrt, 1994: Daytime evolution of relative humidity at the boundary layer top. *Mon. Wea. Rev.*, **122**,

- 2709–2721, [https://doi.org/10.1175/1520-0493\(1994\)122<2709:DEORHA>2.0.CO;2](https://doi.org/10.1175/1520-0493(1994)122<2709:DEORHA>2.0.CO;2).
- , K. E. Mitchell, Y. Lin, E. Rogers, P. Grunmann, V. Koren, G. Gayno, and J. D. Tarpley, 2003: Implementation of Noah land surface model advances in the National Centers for Environmental Prediction operational mesoscale Eta model. *J. Geophys. Res.*, **108**, 8851, <https://doi.org/10.1029/2002JD003296>.
- Erlingis, J. M., and A. P. Barros, 2014: A study of the role of daytime land–atmosphere interactions on nocturnal convective activity in the southern Great Plains during CLASIC. *J. Hydrometeorol.*, **15**, 1932–1953, <https://doi.org/10.1175/JHM-D-14-0016.1>.
- , J. J. Gourley, and J. B. Basara, 2019: Diagnosing moisture sources for flash floods in the United States. Part I: Kinematic trajectories. *J. Hydrometeorol.*, **20**, 1495–1509, <https://doi.org/10.1175/JHM-D-18-0119.1>.
- Findell, K. L., and E. A. B. Eltahir, 2003: Atmospheric controls on soil moisture–boundary layer interactions. Part I: Framework development. *J. Hydrometeorol.*, **4**, 552–569, [https://doi.org/10.1175/1525-7541\(2003\)004<0552:ACOSML>2.0.CO;2](https://doi.org/10.1175/1525-7541(2003)004<0552:ACOSML>2.0.CO;2).
- Gimeno, L., and Coauthors, 2012: Oceanic and terrestrial sources of continental precipitation. *Rev. Geophys.*, **50**, RG4003, <https://doi.org/10.1029/2012RG000389>.
- , and Coauthors, 2016: Major mechanisms of atmospheric moisture transport and their role in extreme precipitation events. *Annu. Rev. Environ. Resour.*, **41**, 117–141, <https://doi.org/10.1146/annurev-environ-110615-085558>.
- Higgins, R. W., Y. Yao, E. S. Yarosh, J. E. Janowiak, and K. C. Mo, 1997: Influence of the Great Plains low-level jet on summertime precipitation and moisture transport over the central United States. *J. Climate*, **10**, 481–507, [https://doi.org/10.1175/1520-0442\(1997\)010<0481:IOTGPL>2.0.CO;2](https://doi.org/10.1175/1520-0442(1997)010<0481:IOTGPL>2.0.CO;2).
- Hu, H., and F. Dominguez, 2015: Evaluation of oceanic and terrestrial sources of moisture for the North American monsoon using numerical models and precipitation stable isotopes. *J. Hydrometeorol.*, **16**, 19–35, <https://doi.org/10.1175/JHM-D-14-0073.1>.
- Jana, S., B. Rajagopalan, M. A. Alexander, and A. J. Ray, 2018: Understanding the dominant sources and tracks of moisture for summer rainfall in the southwest United States. *J. Geophys. Res. Atmos.*, **123**, 4850–4870, <https://doi.org/10.1029/2017JD027652>.
- Koster, R. D., and Coauthors, 2004: Regions of strong coupling between soil moisture and precipitation. *Science*, **305**, 1138–1140, <https://doi.org/10.1126/science.1100217>.
- Luo, Y., E. H. Berbery, K. E. Mitchell, and A. K. Betts, 2007: Relationships between land surface and near-surface atmospheric variables in the NCEP North American Regional Reanalysis. *J. Hydrometeorol.*, **8**, 1184–1203, <https://doi.org/10.1175/2007JHM844.1>.
- Mo, K. C., J. N. Paegle, and R. W. Higgins, 1997: Atmospheric processes associated with summer floods and droughts in the central United States. *J. Climate*, **10**, 3028–3046, [https://doi.org/10.1175/1520-0442\(1997\)010<3028:APAWSF>2.0.CO;2](https://doi.org/10.1175/1520-0442(1997)010<3028:APAWSF>2.0.CO;2).
- Nemunaitis-Berry, K. L., P. M. Klein, J. B. Basara, and E. Fedorovich, 2017: Sensitivity of predictions of the urban surface energy balance and heat Island to variations of urban canopy parameters in simulations with the WRF model. *J. Appl. Meteor. Climatol.*, **56**, 573–595, <https://doi.org/10.1175/JAMC-D-16-0157.1>.
- Nieto, R., L. Gimeno, and R. M. Trigo, 2006: A Lagrangian identification of major sources of Sahel moisture. *Geophys. Res. Lett.*, **33**, L18707, <https://doi.org/10.1029/2006GL027232>.
- Pan, H. L., and L. Mahrt, 1987: Interaction between soil hydrology and boundary-layer development. *Bound.-Layer Meteorol.*, **38**, 185–202, <https://doi.org/10.1007/BF00121563>.
- Robock, A., and Coauthors, 2003: Evaluation of the North American Land Data Assimilation System over the southern Great Plains during the warm season. *J. Geophys. Res.*, **108**, 8846, <https://doi.org/10.1029/2002JD003245>.
- Saharia, M., P. Kirstetter, H. Vergara, J. J. Gourley, Y. Hong, and M. Giroud, 2017: Mapping flash flood severity in the United States. *J. Hydrometeorol.*, **18**, 397–411, <https://doi.org/10.1175/JHM-D-16-0082.1>.
- Skamarock, W. C., and Coauthors, 2008: A description of the Advanced Research WRF version 3. NCAR Tech. Note NCAR/TN-475+STR, 113 pp., <https://doi.org/10.5065/D68S4MVH>.
- Sodemann, H., C. Schwierz, and H. Wernli, 2008: Interannual variability of Greenland winter precipitation sources: Lagrangian moisture diagnostic and North Atlantic Oscillation influence. *J. Geophys. Res.*, **113**, D03107, <https://doi.org/10.1029/2007JD008503>.
- Sorí, R., A. Drumond, and R. Nieto, 2015: Moisture contribution of the Atlantic Warm Pool to precipitation: A Lagrangian analysis. *Front. Environ. Sci.*, **3**, 1–11, <https://doi.org/10.3389/fevs.2015.00022>.
- Stohl, A., and P. James, 2004: A Lagrangian analysis of the atmospheric branch of the global water cycle. Part I: Method description, validation, and demonstration for the August 2002 flooding in central Europe. *J. Hydrometeorol.*, **5**, 656–678, [https://doi.org/10.1175/1525-7541\(2004\)005<0656:ALAOTA>2.0.CO;2](https://doi.org/10.1175/1525-7541(2004)005<0656:ALAOTA>2.0.CO;2).
- , and —, 2005: A Lagrangian analysis of the atmospheric branch of the global water cycle. Part II: Moisture transports between earth's ocean basins and river catchments. *J. Hydrometeorol.*, **6**, 961–984, <https://doi.org/10.1175/JHM470.1>.
- Sun, B., and H. Wang, 2014: Moisture sources of semiarid grassland in China using the Lagrangian particle model FLEXPART. *J. Climate*, **27**, 2457–2474, <https://doi.org/10.1175/JCLI-D-13-00517.1>.
- Trenberth, K. E., and C. J. Guillemot, 1998: Evaluation of the atmospheric moisture and hydrological cycle in the NCEP/NCAR reanalyses. *Climate Dyn.*, **14**, 213–231, <https://doi.org/10.1007/s003820050219>.
- Wei, J., H. R. Knoche, and H. Kunstmann, 2016: Atmospheric residence times from transpiration and evaporation to precipitation: An age-weighted regional evaporation tagging approach. *J. Geophys. Res. Atmos.*, **121**, 6841–6862, <https://doi.org/10.1002/2015JD024650>.
- Xia, Y., and Coauthors, 2013: Validation of Noah-simulated soil temperature in the North American Land Data Assimilation System phase 2. *J. Appl. Meteor. Climatol.*, **52**, 455–471, <https://doi.org/10.1175/JAMC-D-12-033.1>.